Relationship between summer rainfall anomalies and sub-seasonal oscillations in South China

Chunhui Li · Tim Li · Ailan Lin · Dejun Gu · Bin Zheng

Abstract Sub-seasonal variability of summer (May–October) rainfall over South China exhibits two dominant timescales, one with a quasi-biweekly (QBW) period (10–20 days) and the other with an intraseasonal oscillation (ISO) period (20–60 days). A significant positive correlation (at a 99 % confidence level) was found between the summer precipitation anomalies and the intensity of the QBW and ISO modes. By examining the composite structure and evolution characteristics, we note that the QBW and ISO modes are characterized by a northwest-southeast oriented wave train pattern with a pronounced baroclinic vertical structure, moving northwestward. A marked feature is the phase leading of low-level moisture relative to convection. For the QBW mode, such a phase leading feature appears in both the strong and weak composites. However, for the ISO mode, this feature is only clearly seen in the strong composite. The high positive correlation between the summer precipitation and the sub-seasonal variability suggests that the summer mean state may exert a large-scale control on the sub-seasonal modes. It is found that when South China is anomalously wet, large-scale atmospheric conditions in the key QBW/ISO activity region are characterized by deeper moist layer, more convectively unstable stratification, and greater ascending motion. Such environmental conditions favor the growth of the QBW and ISO perturbations.

1 Introduction

Southern China is the region with the greatest mean rainfall in China. The average rain rate in summer (May–October) exceeds 10 mm/day (Fig. 1a). The climate in South China exhibits a typical monsoon characteristic, with clear dry and wet seasons. Two peaks appear in the wet summer season in June and August, respectively, as revealed from the annual cycle over South China (Fig. 1b). Floods occur more frequently during the early summer (May–June), accounting for about 40–50 % of annual rainfall (Lu 1990). In late summer (July–September), precipitation is often related to typhoons and tropical waves.

Summer rainfall in South China also experiences a great year-to-year and interdecadal variations (Chang et al. 2000a; Wu et al. 2010; Li et al. 2011; Wu et al. 2012). Figure 1c shows that the standard deviation of the summer rain rate interannual variability is 2 mm/day. A number of factors may contribute to the interannual variation of rainfall over South China. They include the subtropical high (Liang 1994; Qin et al. 1994; Deng and Wang 2002), the El Nino-southern Oscillation (Chang et al. 2000a, b), Sea Surface Temperature (SST) in surrounding oceans (Guo and Sha 1998; Gao et al. 1999), Tibetan Plateau snow cover (Cai et al. 2000), Southern Hemispheric pressure systems (Zhang et al. 1997; Xue et al. 2003), Antarctic sea ice (Wu et al. 1998) and the South China Sea monsoon (Li et al. 1995; Liang and Wu 1999).

C. Li (✉) · A. Lin · D. Gu · B. Zheng
Institute of Tropical and Marine Meteorology/Guangdong Provincial Key Laboratory of Regional Numerical Weather Prediction, China Meteorological Administration, Guangzhou 510080, China
e-mail: chli@grmc.gov.cn

T. Li
IPRC and Department of Meteorology, University of Hawaii, Honolulu, HI, USA

Fig. 1 a 50-year (1958–2007) climatologic rain rate averaged from May to October (unit: mm/day) in China, **b** Climatologic annual cycle of rain rate averaged over the South China box (107°–120°E, 21°–27°N) (unit: mm/day), **c** The standard deviation of interannual variation of May–October rain rate (unit: mm/day), and **d** the 50-year average of standard deviation of the 10–60-day filtered rain rate (unit: mm/day) over 743 weather stations over China
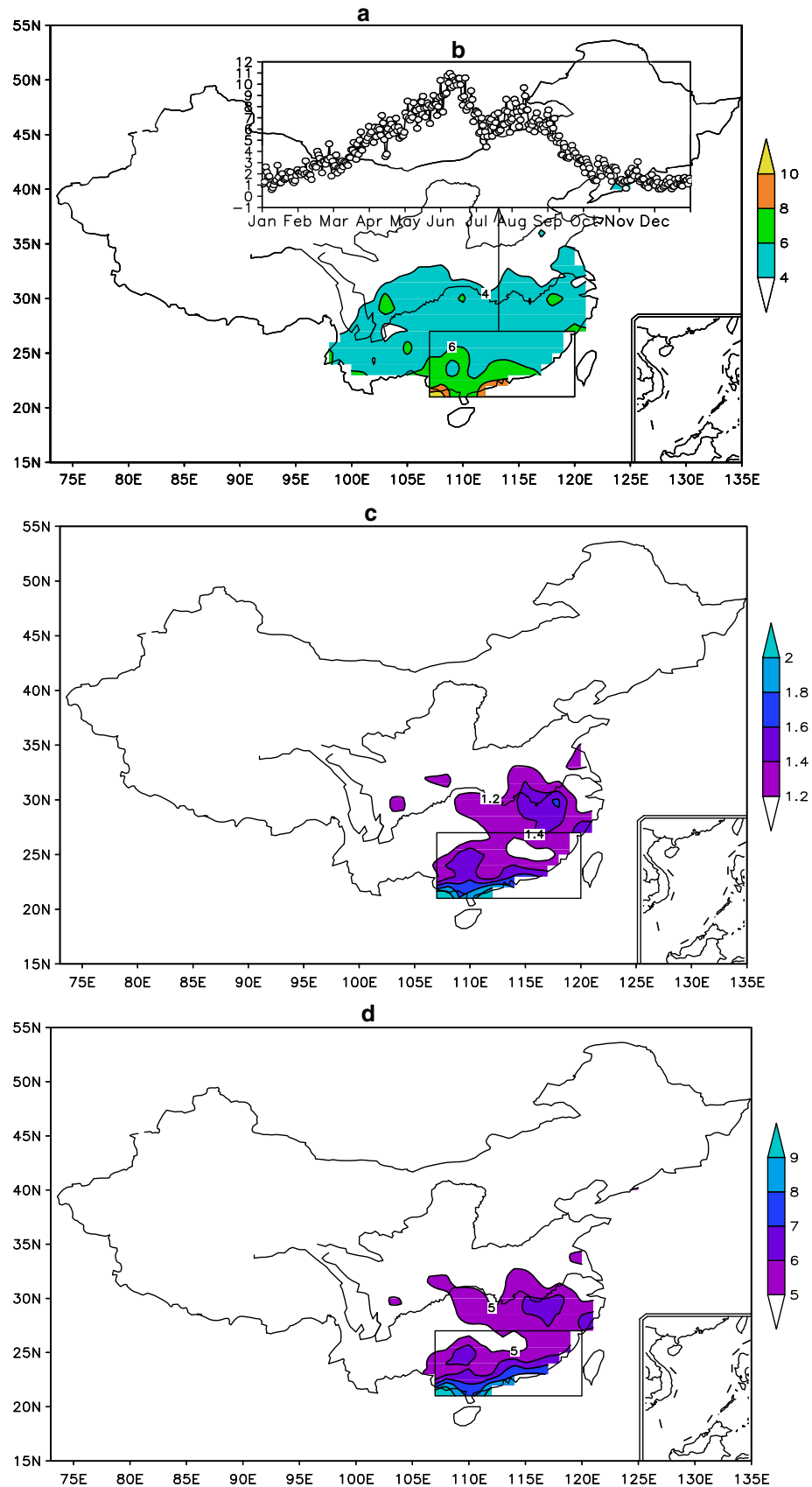
In addition to the interannual variability, rainfall over South China also has a strong sub-seasonal variation (Fig. 1d). Two major sub-seasonal modes have been widely recognized over the region during boreal summer: the quasi-biweekly mode (QBW) and the lower-frequency intraseasonal oscillation (ISO) mode (Li and Wang 2005). The former is characterized by westward or northwestward propagation, originated from the tropical western Pacific, with a typical period of 10–20 days (Krishnamurti and Ardanuy 1980; Chen and Chen 1995; Annamalai and Slingo 2001; Mao and Chan 2005; Kajikawa and Yasunari 2005; Yang et al. 2008). The latter is characterized by northward propagation, with a dominant period of 30–60 days (Chen and Murakami 1988; Hsu and Weng 2001; Kemball-Cook and Wang 2001; Lawrence and Webster 2002; Hsu et al. 2004).

There is a controversy on the mean rainfall-ISO relationship. Li et al. (1995) found a negative relationship, that is, when the tropical ISO in the South China Sea (SCS) is strong, the seasonal mean rainfall anomaly over South China is negative, and vice versa. Shi and Ding (2000), however, noted that the wet summer monsoon in 1994 is accompanied by a greater 30–60-day oscillation. A persistent heavy rainfall event in June 2005 in South China was attributed to continuously northwestward propagation of low frequency convective systems (Wen et al. 2007; Lin et al. 2007). Note that most of the aforementioned studies were case studies. It is necessary to reveal the long-term statistical relationship between the summer mean rainfall anomaly and the sub-seasonal oscillation modes.

The objective of this study is to document, based on a relatively long station rainfall record (1958–2007), the relationship between the summer rainfall anomaly and strength of the QBW and ISO modes in South China, and to reveal possible mechanisms responsible for such a relationship. The rest of the paper is organized as below. In Sect. 2, we describe the data and methods used. In Sect. 3 we first reveal the summer rainfall—QBW/ISO relationship, and then examine the structure and evolution characteristics of the QBW and ISO modes associated with the wet and dry summers in South China. In Sect. 4, we further examine the possible role of large-scale circulation patterns associated with the wet and dry summers in determining the strength of the QBW and ISO modes. Finally a summary and discussion are given in Sect. 5.

2 Data and methods

The primary data used in this study include (1) NCEP global $2.5° \times 2.5°$ monthly mean reanalysis dataset that consists of 3-dimensional temperature, geopotential height and wind fields from 100 to 1000 hPa for the period of 1958–2007, (2) precipitation measured from 743 weather stations across China for the same period (1958–2007), provided by the National Climate Center of China, and (3) reconstructed ERSST sea surface temperature data (Smith and Reynolds 2003, 2004) at a $2° \times 2°$ horizontal resolution (ftp.ncdc.noaa.gov/pub/data/ersst-v2/).

A Lanczos band-pass filtering (Trenberth 1984) is used to isolate the QBW (10–20-day) and ISO (20–60-day) components from original raw data. The selection of the two frequency bands is mainly based on a power spectra analysis (Bingham et al. 1967) of the daily precipitation data averaged in the South China box (107°E–120°E and 21°–27°N, shown in Fig. 1) for the summer period from 1978 to 2007 (when satellite observations became available) (Fig. 2). Figure 2 shows clearly that both 10–20-day variability and 20–60-day variability are statistically significant. Here statistical significance of power spectra was tested following Gilman et al. (1963) according to the power spectrum of mean red noise.

Throughout the paper the summer is referred to as a period from May to October base on the study of Li and Wang (2005), who showed that the cross patterns of QBW and ISO modes are quite similar between earlier (MJJ) and later (ASO) summer. The interannual variability of summer rainfall over South China is measured by the rainfall amount during the summer period averaged over the region of (107°E–120°E and 21°–27°N). A composite analysis method is used to reveal either the mean circulation feature or the structure and evolution characteristics associated with the QBW and ISO modes. A student t-test is applied to examine the statistical significance of the differences between two composite groups.

3 Composite structure and evolution characteristics of the QBW and ISO modes during strong and weak years

Figure 3 shows the time series of the summer rain rate anomalies and the QBW/ISO intensity anomalies from 1958 to 2007. Here the QBW and ISO intensity is defined by the standard deviation of 10–20-day and 20–60-day filtered rain rate fields each summer. Note that there is a high positive correlation between the QBW/ISO intensity and the summer rain rate anomaly. The correlation coefficient between the summer rain rate and the QBW intensity is 0.78, and the correlation coefficient between the summer rain rate and the ISO intensity is 0.74, both of which are beyond the 0.01 significance level. If separating the earlier (MJJ) and later (ASO) summer, one may find that significant (exceeding 95 % confidence level) positive correlations between the mean rain rate and QBW/ISO
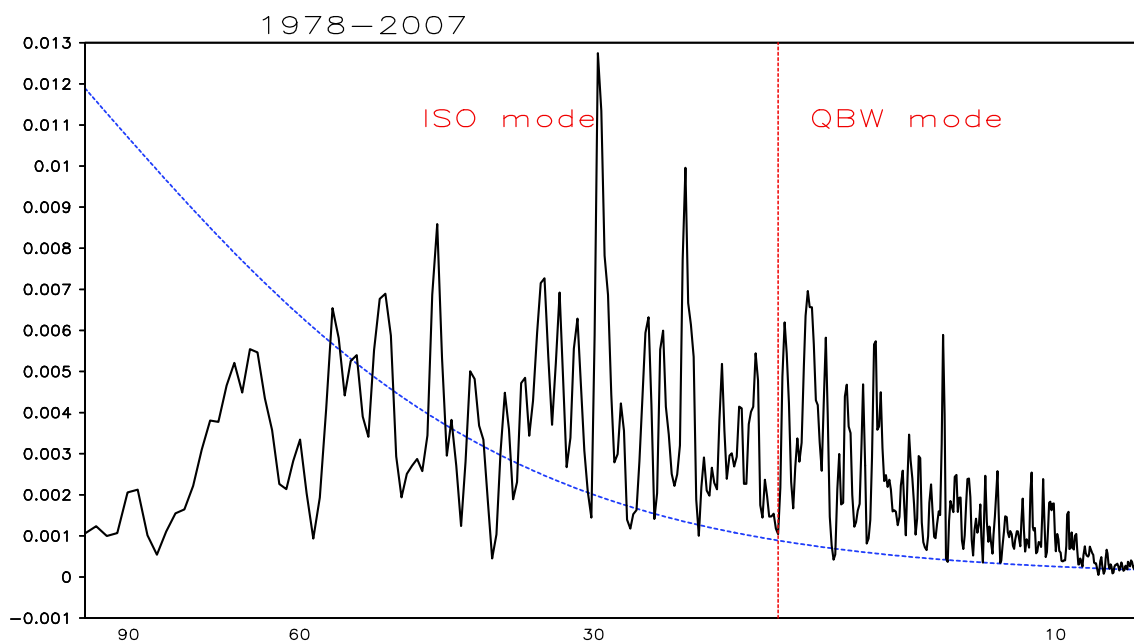
Fig. 2 Power spectrum of observed daily precipitation time series averaged in the South China box (107°E–120°E and 21°–27°N) for the summer (May–Oct) period from 1978 to 2007. The *blue dash line* represents the 95 % confidence level. The *red dash line* separates the QBW and ISO mode
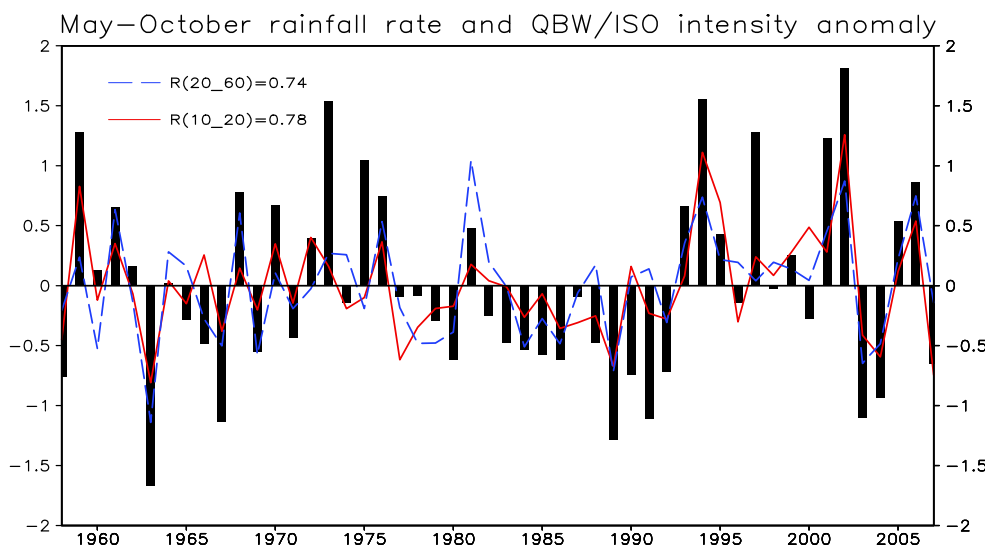

Fig. 3 Time evolutions of the May–October rain rate anomaly (bar, unit: mm/day) and the intensity anomaly (unit: mm/day) of the QBW (*red*) and ISO modes (*blue*) averaged over the South China box (107°–120°E, 21°–27°N). For vertical axis, the *left* one is for the May–October rain rate anomaly and the *right* one is for the QBW/ISO intensity anomaly. *R* values in the *top left corner* denote temporal correlation coefficients between the May–Oct rain rate anomaly time series and the time series of the QBW/ISO intensity anomaly

intensity exist in both the periods (see Table 1). This high positive correlation is in contrast to a negative ISO-summer mean rainfall correlation over South Asia (Qi et al. 2008). A time filtering method (based on a band-pass filter analysis) is applied to isolate the interdecadal (longer than 9 year) and interannual (2–9 year) timescales. Our results show that the large correlation coefficients between the

Table 1 Correlation coefficients between the average rain rate and the QBW/ISO intensity in earlier summer (MJJ) and later summer (ASO)

	May–July	August–October
<QBW, rain>	0.57	0.58
<ISO, rain>	0.55	0.56

Table 2 Correlation coefficients between the May–Oct rain rate and the QBW/ISO intensity in the South China box on interannual (2–9 year) and interdecadal (>9 year) timescales

	Interannual timescale	Interdecadal timescale
<QBW, rain>	0.78	0.70
<ISO, rain>	0.75	0.65

QBW/ISO intensity and summer rain rate are primarily attributed to the interannual component (Table 2).

Significant positive correlations above suggest that the summer mean flow may play an important role in modulating the QBW and ISO modes. Before investigating how the mean flow influences the sub-seasonal oscillations, we first examine the composite structure and evolution characteristics of the QBW and ISO modes. Strong (weak) years of the QBW and ISO modes are selected when the QBW and ISO intensity indices exceed 1 (−1) standard deviation. Figure 4 shows the evolution (from day −6 to day 0) of the composite QBW mode pattern during strong and weak years. Here day 0 is a reference time when the rainfall anomaly associated with the QBW mode reaches a maximum over South China, and the strong (weak) years are those when the QBW strength exceeds positive (negative) one standard deviation. During the strong QBW years (left panel), an anomalous cyclone appears over Philippines (about 15°N) at day −6. Meanwhile, an anomalous anticyclone and negative rainfall anomalies appear over South China. The dominant structure of the QBW mode is a northwest-southeast oriented wave train, with a half wavelength of about 10–15° in longitude. In the following days, the anomalous anticyclone in South China decreases gradually as the wave train moves northwestward. The anomalous cyclone to its south intensifies gradually and moves to about 20°N at day −4 and 23°N at day −2. Meanwhile, a new anticyclone anomaly forms to its south. At day 0, the anomalous cyclone reaches its maximum intensity as it arrives in South China, resulting in a large rainfall anomaly. The northwestward propagation occurred mainly between day −6 day and −2. The perturbation became stationary and dissipated after day 0. A marked feature of the QBW mode is that over the tropical ocean the wave train continues to move northwestward as new disturbances are generated over the Philippine Sea.

Compared to the strong years, the QBW disturbance during the weak years also shows a northwest–southeast oriented wave train structure, but the wave train is weaker and less organized. The wavelength also appears smaller.

To clearly show propagation feature, we plotted the meridional -time distribution of 850 hPa and 200 hPa vorticity averaged over 107°E–120°E (Fig. 5). The most evident difference between the strong and weak year composites in the lower troposphere lies in the timing and latitudinal location of the initial perturbation. During the strong QBW years, the positive vorticity anomalies develop earlier (at day −8) and start from a more southern position (about 10°N). During the weak QBW years, the positive vorticity anomalies develop later (at day −4) and start from a more northern position (about 20°N). Regardless strong or weak years, lower (850 hPa) and middle (500 hPa, figure not shown) tropospheric vorticity perturbations show consistent northward propagation. This is in contrast to the upper-tropospheric (200 hPa) perturbations, which exhibit an opposite propagation direction between the strong and weak composites. In the former the vorticity perturbations propagate northward (Fig. 5c), whereas in the latter they propagate southward (Fig. 5d).

The zonal-time cross sections of the QBW vorticity perturbations averaged over 21°N–27°N are shown in Fig. 6. There are consistent westward propagating signals in the lower (850 hPa) and middle (500 hPa, figure not shown) troposphere during both the strong and weak years. The difference between strong and weak years lies in the longitudinal extension of the perturbation. In the former the QBW perturbation can start from a further eastern position (about 135°E), whereas in the weak years, the QBW perturbation starts from a more western position (about 125°E). No obvious vorticity propagation was observed in the upper troposphere (200 hPa) during both the strong and weak years (Fig. 6c, d).

Figure 7 illustrates the vertical-time cross sections of the QBW vertical velocity, specific humidity and vorticity fields averaged over South China (107°E–120°E, 21°N–27°N) during the strong and weak years. The most pronounced feature associated with the QBW mode is the phase leading of specific humidity in the lower troposphere. Two or three days prior to local rainfall maximum, a low-level moisture anomaly center appears. This implies that the low-level moisture associated with the QBW mode leads the convection during its northwestward movement. Such a feature appears in both the strong and weak composites, although the amplitude of the moisture anomaly is greater in the strong composite. Another interesting feature is the baroclinic structure of the vorticity perturbation. A positive vorticity anomaly in the lower troposphere is accompanied with a negative vorticity anomaly in the upper troposphere. The temporal evolution of the vorticity perturbation appears different between the strong and weak composites. During the strong years, a positive vorticity anomaly in the upper troposphere leads the lower-tropospheric vorticity anomaly, implying a downward development. During the weak QBW years, upper-tropospheric vorticity lags the low-tropospheric vorticity, implying an upward development.
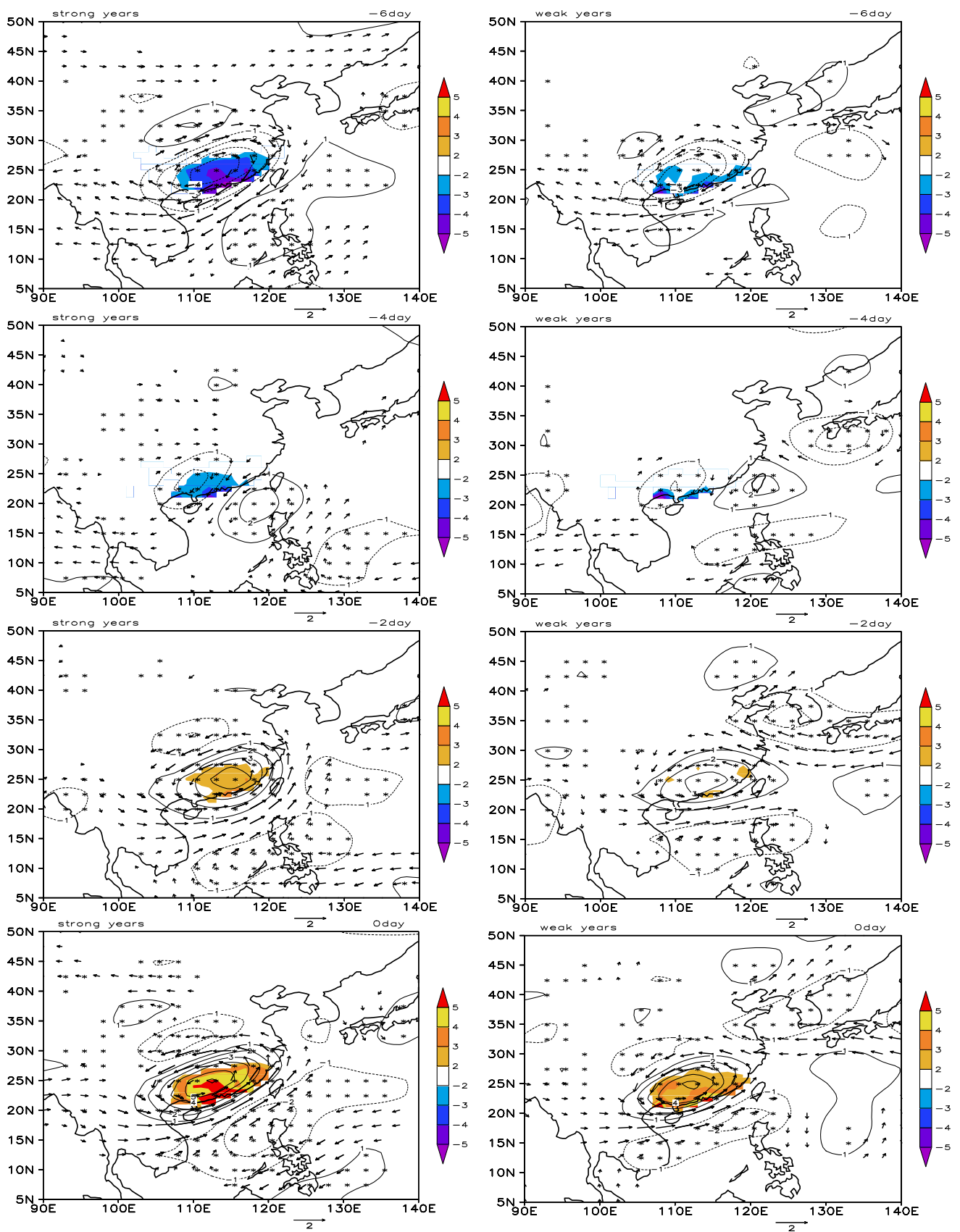
◀**Fig. 4** Composite evolution of 850 hPa wind (vector, unit: m s^{-1}, areas exceeding a 95 % confidence level were plotted), vorticity (contour, unit: 10^{-5} s^{-1}, *asterisk* symbol shows the 95 % confidence level or above) and rainfall (*shaded*, unit: mm/day, areas that exceed a 95 % confidence level were plotted) associated with the QBW mode from day −6 to day 0 during the strong (*left*) and weak (*right*) QBW years. Day 0 denotes a reference time when the QBW rainfall anomaly reaches maximum intensity over South China

The baroclinic vorticity anomaly is in phase with the perturbation vertical motion (Fig. 7). The vertical profile of the vertical motion shows a maximum ascending center in the middle troposphere. Associated with this ascending motion are the low-level convergence and the upper-tropospheric divergence anomalies (figure not shown). Thus, the in-phase vertical motion-vorticity relationship implies that the generation of the perturbation vorticity is primarily attributed to the divergence-related stretching term. It is also noted that the ascending motion is associated with enhanced southerly (northerly) anomalies in the lower (upper) troposphere.

A parallel analysis was done for the 20–60-day mode. The composites here were based on strong and weak ISO years. Figure 8 illustrates the time sequence maps of the composite rainfall and 850-hPa wind and vorticity fields during the strong and weak ISO years. A similar northwest-southeast oriented wave train dominates in the East Asia-western Pacific region. At day −15, a large-scale cyclonic circulation appears over the South China Sea and the western Pacific (about 15°N); a negative rainfall anomaly, accompanied by an anomalous anticyclonic circulation, appears over South China. In the following days, the anticyclone decreases gradually and moves northwestward, while the cyclone intensifies gradually and moves northward. The anomalous cyclonic circulation reaches about 17.5°N at day −10 and 23°N at day −5. Meanwhile, a new anticyclone anomaly forms over the South China Sea. At day 0, the cyclone arrives at South China and reaches its maximum intensity, resulting in abundant rainfall. Such a feature is similar to the QBW mode.
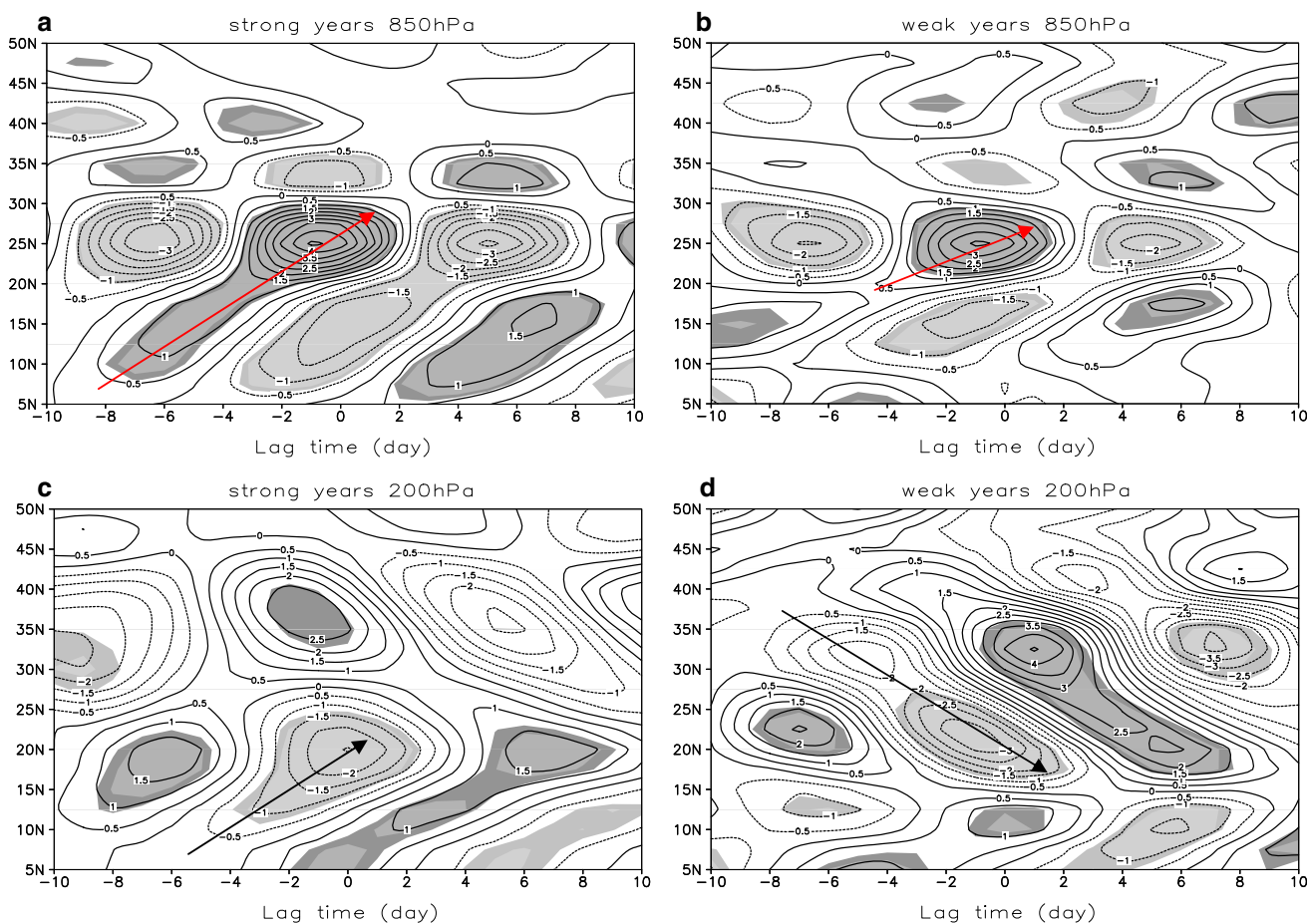

Fig. 5 Meridional-time section of the QBW vorticity (unit: 10^{-5} s^{-1}, areas exceeding the 95 % confidence level were *shaded*) at 850 hPa (*top*) and 200 hPa (*bottom*) along 107°E–120°E. The composite was made based on strong (*left*) and weak (*right*) QBW years. Lagged day 0 denotes a time when the QBW rainfall anomaly reaches maximum over South China
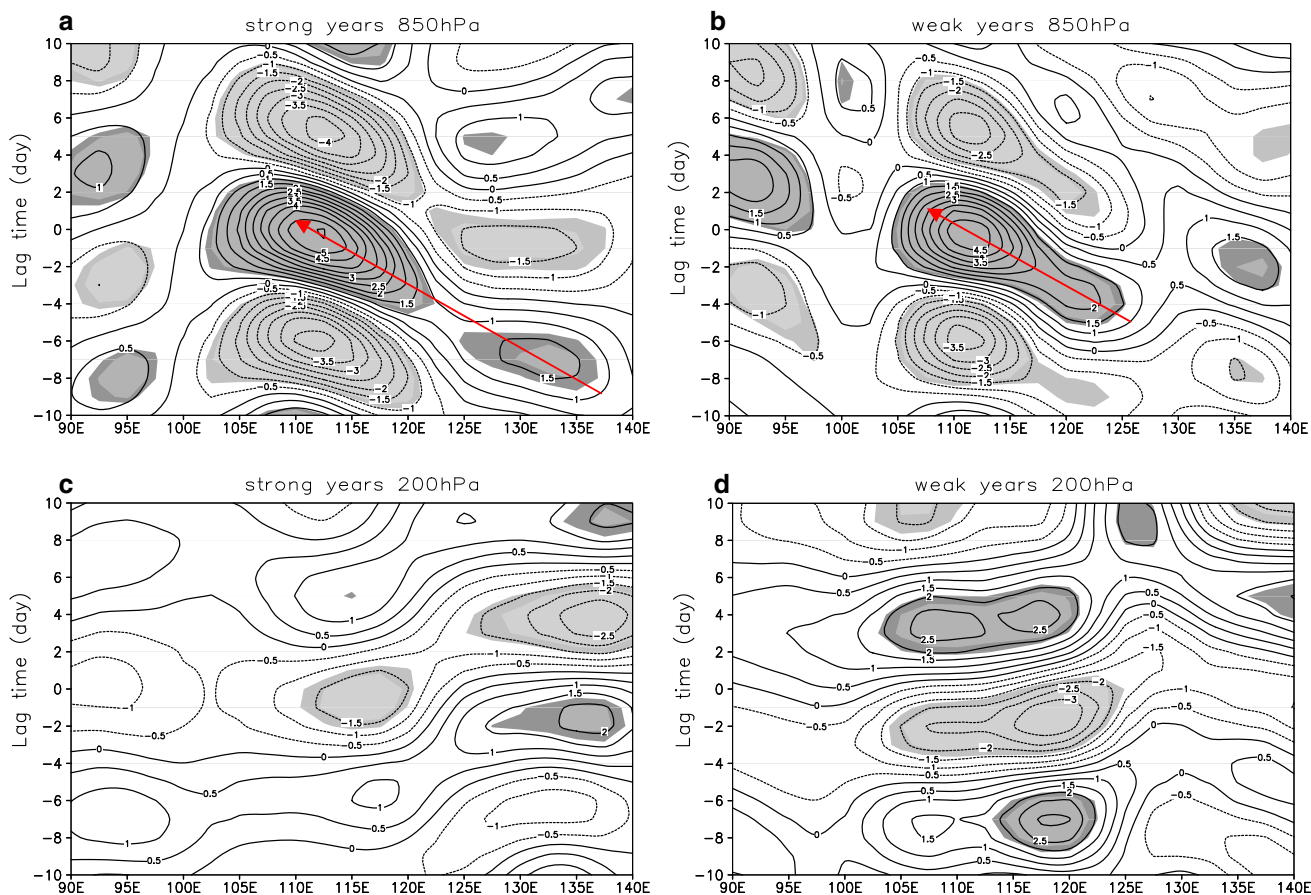
Fig. 6 Zonal-time sections of the QBW vorticity (units: 10^{-5} s^{-1}, areas exceeding the 95 % confidence level were *shaded*) at 850 hPa (*top*) and 200 hPa (*bottom*) averaged along 21°N–27°N. The composite was made based on strong (*left*) and weak (*right*) QBW years. Lagged day 0 denotes a time when the QBW rainfall anomaly reaches maximum over South China

A similar evolution pattern appears during the weak ISO years, compared to that during the strong years. The major difference lies in the amplitude of perturbations (Fig. 8).

The meridional-time distribution of the ISO vorticity perturbation averaged over 107°E–120°E is shown in Fig. 9. The most evident difference between the strong and the week ISO years is in the precursor signal in the upper troposphere. During the strong ISO years, local vorticity perturbation over South China is influenced by signals from both the North and the South (Fig. 9c). During the weak ISO years, the vorticity perturbations always propagate northward (Fig. 9d). In the lower (850 hPa) and middle (500 hPa) troposphere, the vorticity perturbation signals always propagate northward, regardless of strong and weak ISO years. The difference between them lies primarily in the amplitude and latitudinal extent of the perturbation.

The zonal-time distribution of the ISO vorticity perturbation averaged over 21°N–27°N is shown in Fig. 10. While the low-level vorticity perturbation shows the same westward propagation characteristic (Figs. 10a, 10b), the amplitude and longitudinal extent of the perturbations differ between the strong and weak years. During the strong ISO

years, the signal can extend to east of 140°E, whereas during the weak years, the vorticity signal is confined to the west of 130°E. A similar propagation feature is found in the middle troposphere (500 hPa, figure not shown). However, no obvious meridional propagation signals were observed in the upper troposphere (Fig. 10c, d).

The vertical structures of the ISO mode (Fig. 11) in general resemble those of the QBW mode. A major difference lies in the specific humidity field. A phase leading of low-level specific humidity to the rainfall center is clearly seen in the strong ISO composite, but not so in the weak ISO composite. Different from the QBW mode, the upper-tropospheric vorticity perturbation associated with the ISO mode always leads the lower-tropospheric vorticity in both the strong and weak composites.

The diagnosis above is based on strong and weak QBW/ISO year composites. For comparison, we also performed the same diagnosis using the summer rainfall anomalies as a criterion (i.e., defining a wet or a dry year based on whether rainfall anomalies exceed a standard deviation). It turns out that the result is quite similar (figure not shown). This is consistent with the fact that the correlation between
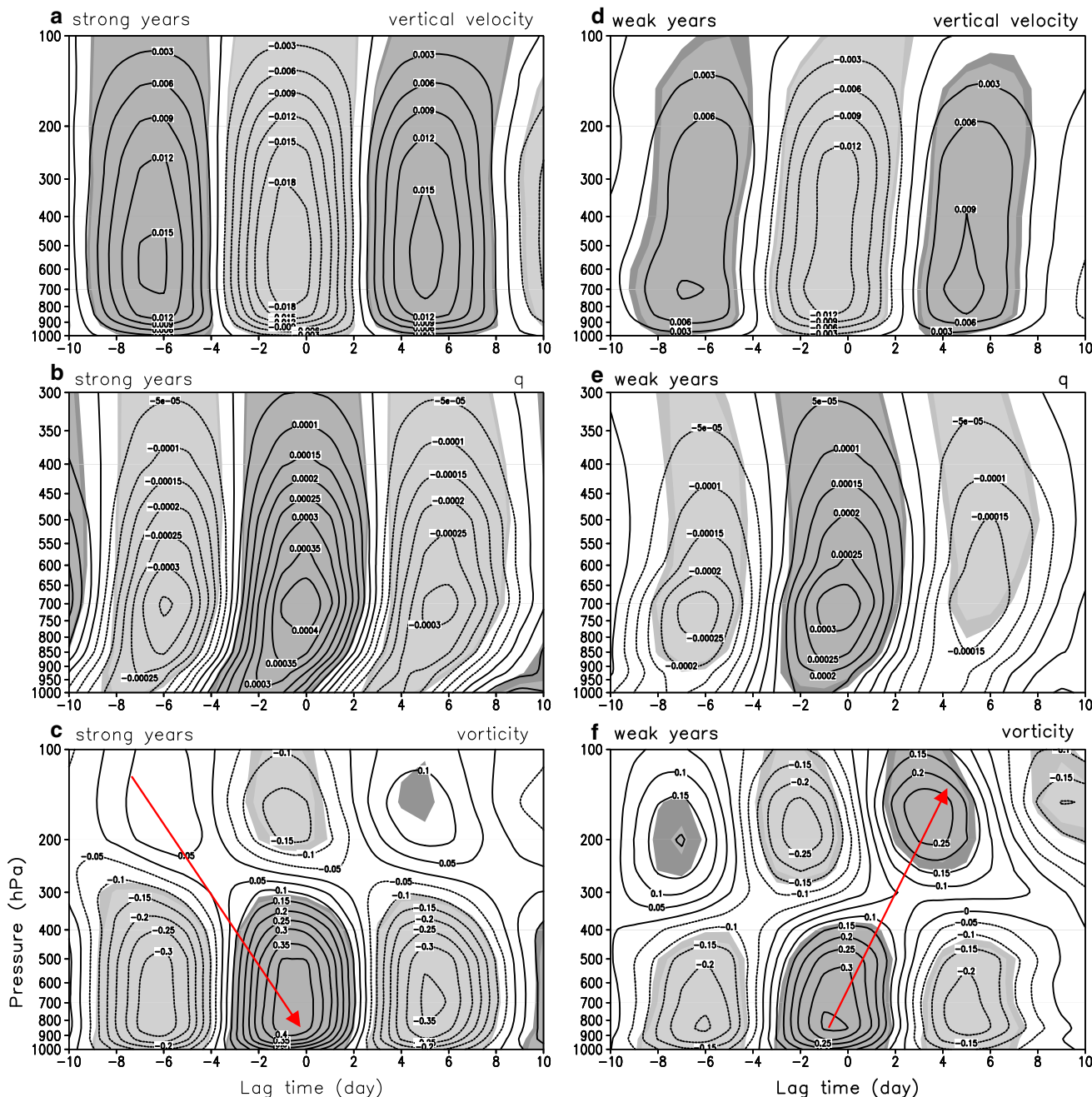
Fig. 7 Vertical-time sections of composite vertical velocity (*top*, unit: 10^{-3} Pa s^{-1}), specific humidity (*middle*, unit: g/kg), vorticity (*bottom*, unit: 10^{-5} s^{-1}) averaged over the South China box (107°E–120°E, 21°N–27°N) during strong (*left*) and weak (*right*) QBW years.

Lagged day 0 denotes a time when the QBW rainfall anomaly reaches maximum over South China. Areas exceeding the 95 % confidence level were *shaded*

the summer rainfall anomaly and the intensity of QBW and ISO is quite high, exceeding 99 % confidence level.

4 Effect of the mean state on sub-seasonal variability

The high positive correlation between the summer precipitation anomaly and the QBW/ISO strength suggests that

the mean flow in the East Asia monsoon region may play an important role in regulating the QBW and ISO activity. As seen from Figs. 4 and 8, the QBW and ISO modes are most active over the South China Sea and Philippine Sea region (10°–25°N, 110°–130°E). Because of that, in the following we will focus on examining the mean flow difference between the wet and dry years in the region. The wet and dry years are defined when the summer rainfall
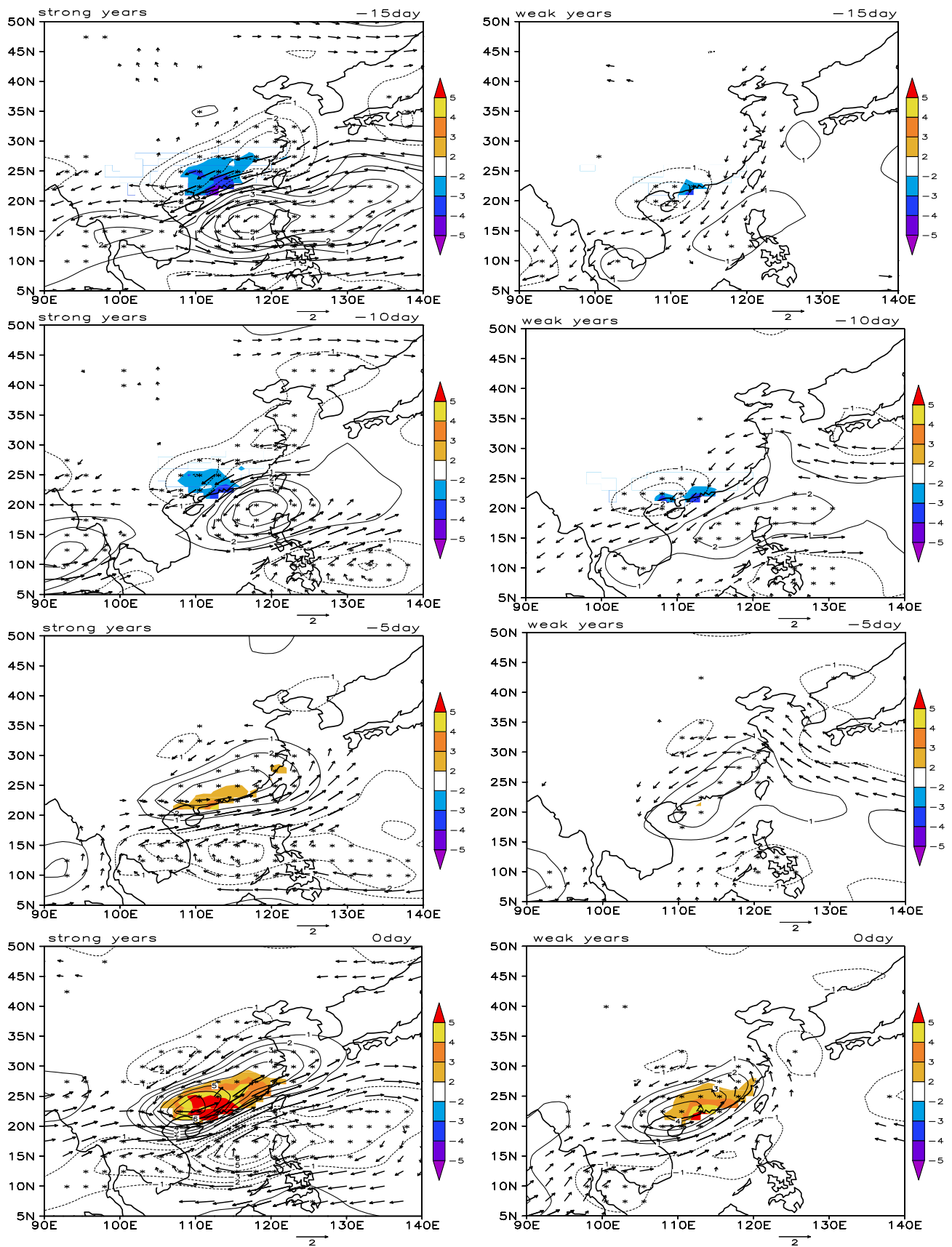
Fig. 8 Composite evolution of 850 hPa wind (vector, unit: m s^{-1}, areas exceeding the 95 % confidence level were plotted), vorticity (contour, unit: 10^{-5} s^{-1}, *asterisk* symbol shows the 95 % confidence level or above) and rainfall (*shaded*, unit: mm day^{-1}, areas exceeding the 95 % confidence level were plotted) associated with the ISO mode from day −15 to day 0 during the strong (*left*) and weak (*right*) ISO years. Day 0 denotes a reference time when the ISO rainfall anomaly reaches maximum intensity over South China

anomaly exceeds positive and negative one standard deviation. According to this definition, seven wet years were selected. They are 1959, 1973, 1975, 1994, 1997, 2001 and 2002. Six dry years were selected. They are 1963, 1967, 1989, 1991, 2003 and 2004.

Figure 12a illustrates the different patterns of composite 850-hPa wind and 700 hPa specific humidity fields between the wet and dry years. The dominant pattern is anomalous low-level cyclonic circulation over South China with increasing lower-tropospheric water vapor over the QBW/ISO development region. An anomalous anticyclone center is located in the western Pacific (at 140°E, 15°N). The anomalous circulation associated with the anticyclone

transports warm and wet air from the surrounding ocean into the development region, causing the increase of moisture in situ. This moisture transport effect can be further revealed later from the regional moisture flux convergence field. In the upper troposphere (200 hPa, Fig. 12b), a divergence center is located over South China.

The composite SST and OLR difference maps (Fig. 12c) show that during the concurrent summer (May–October), a positive SST anomaly appears in the South China Sea, while a negative SST anomaly appears in the western North Pacific. The averaged OLR anomaly over the QBW/ISO development region is negative, indicating that this is the region of enhanced mean convection. It appears that the anomalous anticyclone in the western North Pacific is a Rossby wave response to a negative diabatic heating anomaly associated with the local cold SSTA (Gill 1980). The cold SSTA and the anomalous anticyclone co-existed in the western North Pacific in the preceding spring and winter, suggesting that a positive local thermodynamic air-sea feedback was involved (Wang et al. 2003).
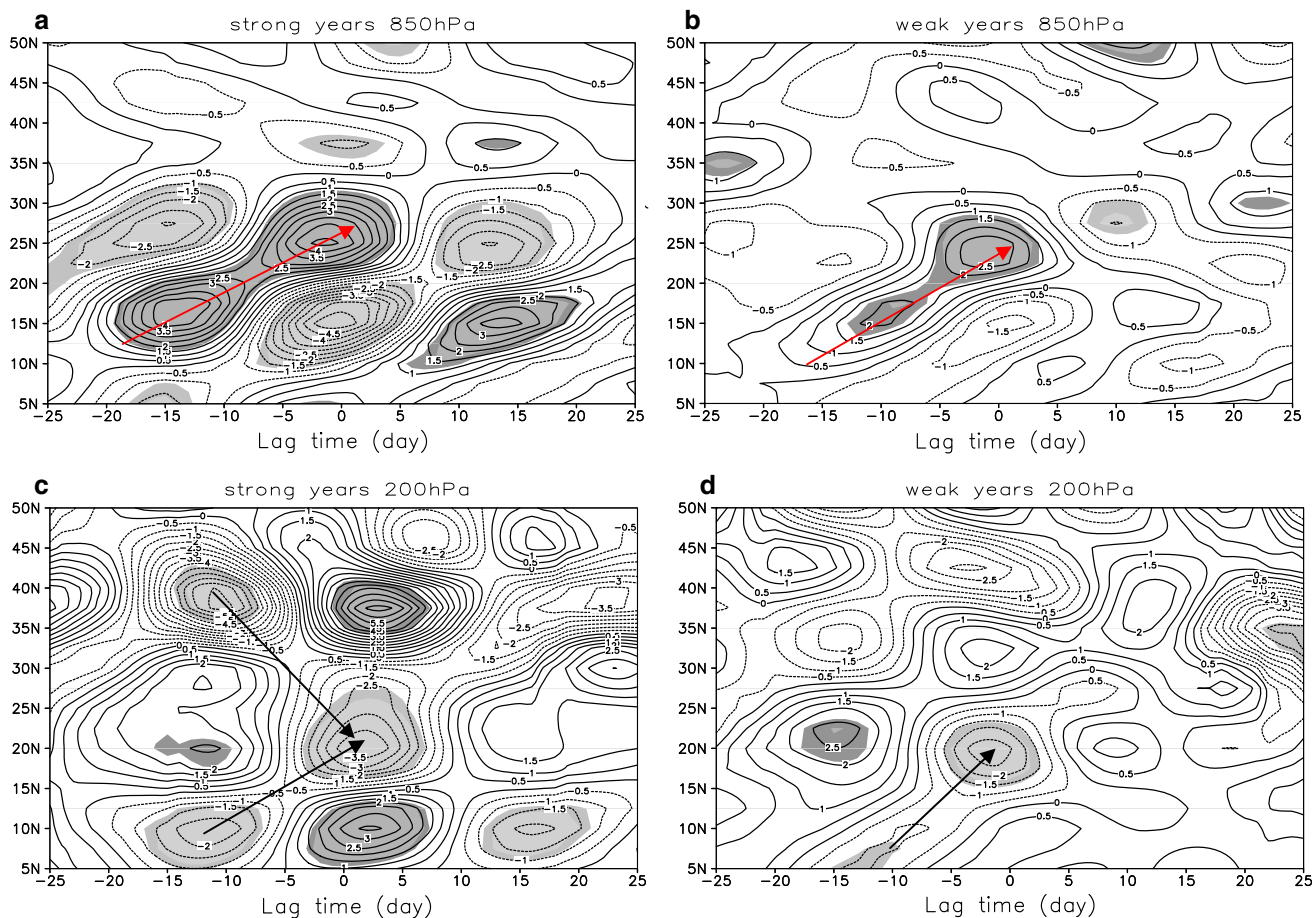

Fig. 9 Meridional-time section of the ISO vorticity (unit: 10^{-5} s^{-1}, areas exceeding the 95 % confidence level were shaded) at 850 hPa (*top*) and 200 hPa (*bottom*) along 107°E–120°E. The composite was made based on strong (*left*) and weak (*right*) ISO years. Lagged day 0 denotes a time when the ISO rainfall anomaly reaches maximum over South China
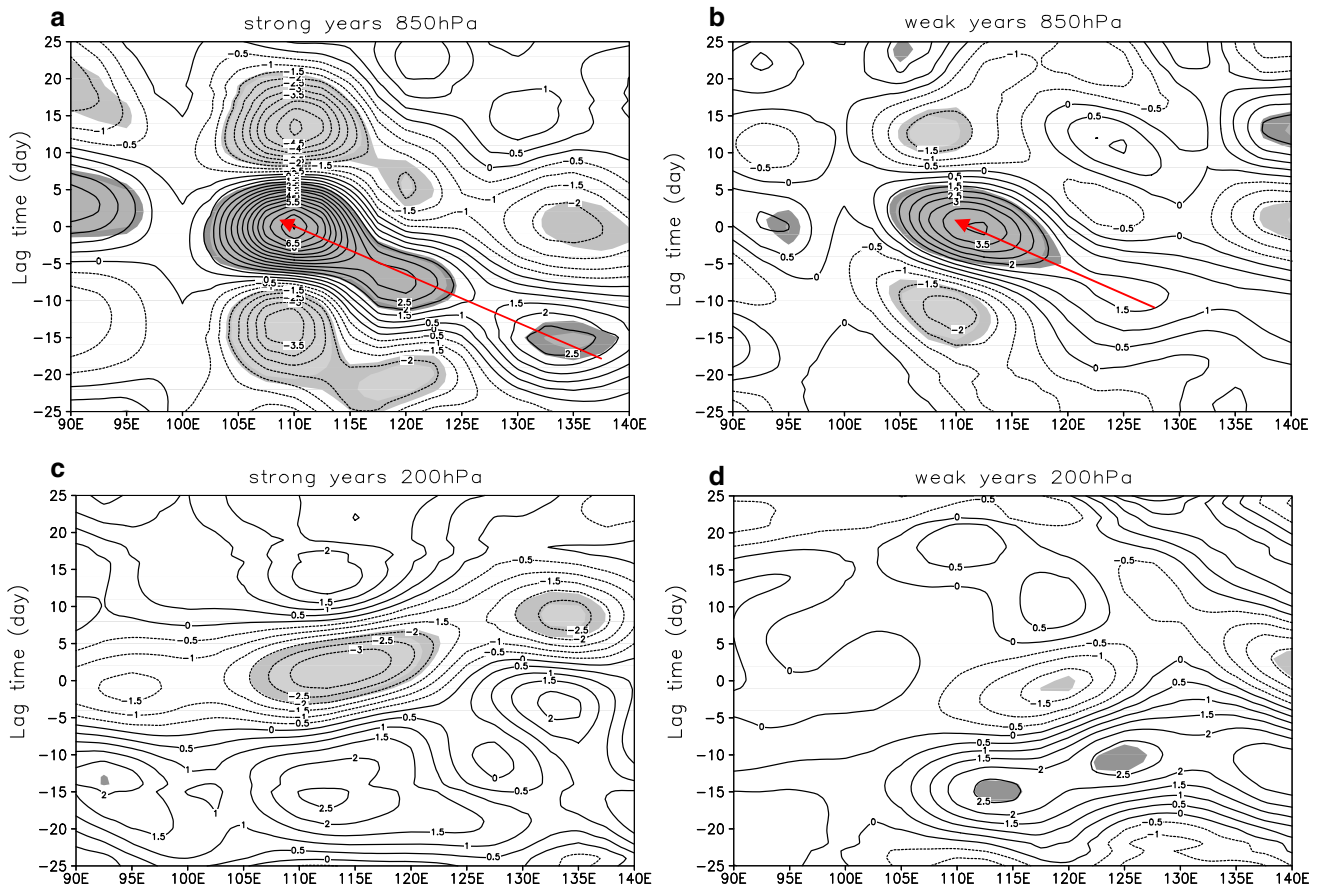
Fig. 10 Zonal-time sections of the ISO vorticity (units: 10^{-5} s^{-1}, areas exceeding the 95 % confidence level were shaded) at 850 hPa (*top*) and 200 hPa (*bottom*) averaged along 21°N–27°N. The composite was made based on strong (*left*) and weak (*right*) ISO years. Lagged day 0 denotes a time when the ISO rainfall anomaly reaches maximum over South China

To focus on the key QBW/ISO development region, we plotted the vertical profiles of the area averaged summer mean temperature, specific humidity, moist static energy, equivalent potential temperature, vertical p-velocity, divergence, relative humidity, and moisture flux convergence fields. All quantities above were averaged over the region of (10°–25°N, 110°–130°E) for both the wet and dry years, and they are anomalous vertical profiles as the long-term climatological mean profiles have been removed. From the temperature profile (Fig. 13a), one can see clearly that during the wet years, the atmosphere is warmer (colder) in the lower (upper) troposphere so that the atmosphere is more statically unstable. The specific humidity profile (Fig. 13b) shows that the lower troposphere is more humid in the wet years; as a result, the atmosphere is more convectively unstable, as it is seen in the moist static energy and equivalent potential temperature profiles (Figs. 13c, d). The cause of the more humid air column during the wet years is partly attributed to anomalous ascending motion (Fig. 13e), which transports the mean moisture upward. Associated with the pronounced ascending motion is anomalous convergence (divergence)

at the lower (upper) troposphere (Fig. 13f). The enhanced low-level convergence may increase local moisture through the low-level moisture flux convergence (Fig. 13h).

It is argued that the summer mean conditions such as more convectively unstable stratification and anomalous ascending motion in the QBW/ISO development region during the wet years may favor the growth of tropical low-frequency perturbations (Li and Wang 2005; Hsu and Li 2011). The enhanced ISO strength may further modulate synoptic wave and TC activity (Liebmann et al. 1994; Zhou and Li 2010; Hsu et al. 2011). This explains why the observed intensity of the QBW and ISO modes is positively correlated with the summer mean monsoon precipitation over South China.

5 Summary and discussion

The characteristics of interannual variations of sub-seasonal modes in boreal summer (May–October) and their relationship with the summer rainfall anomalies in South
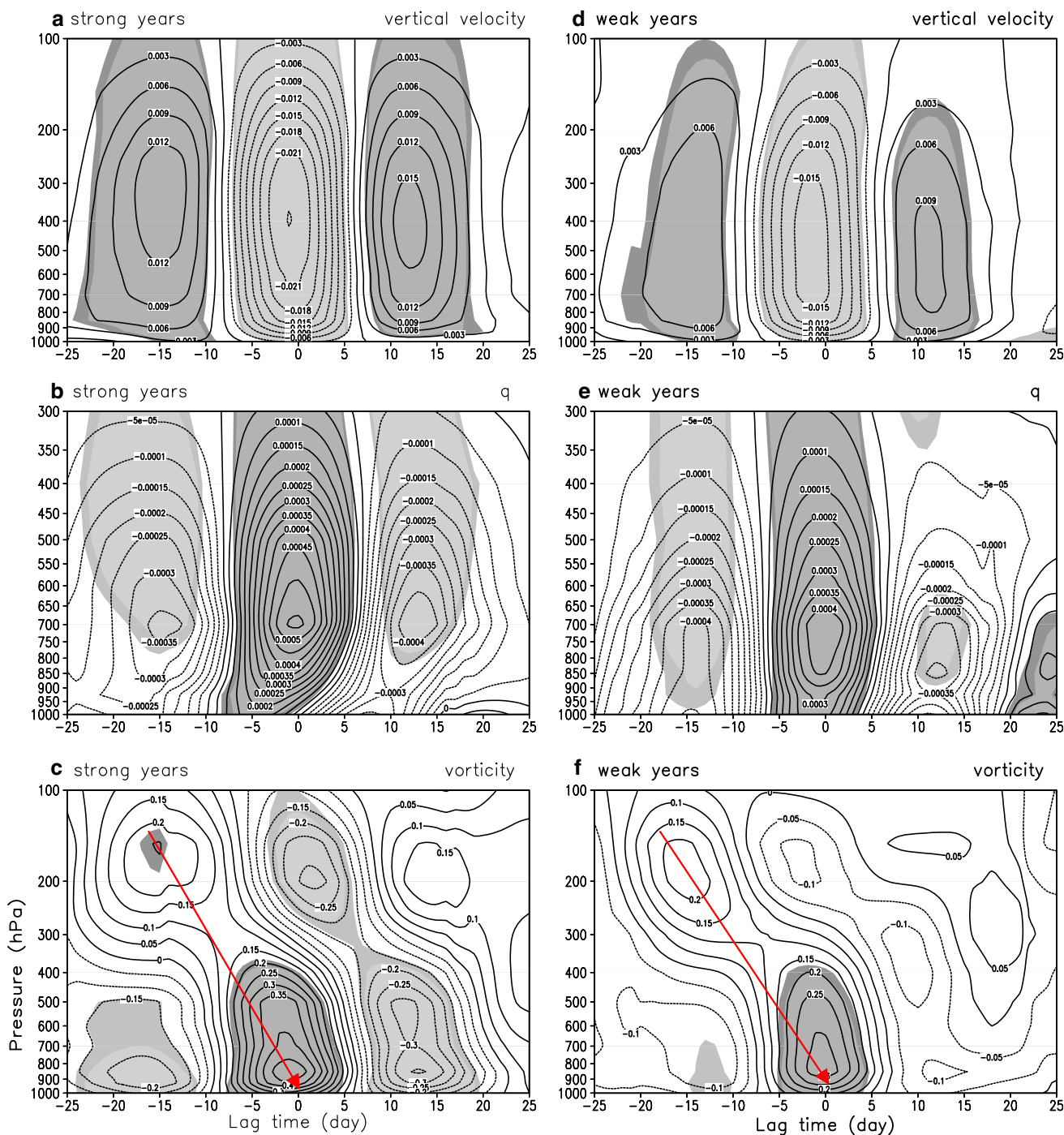
Fig. 11 Vertical-time sections of composite vertical velocity (*top*, unit: 10^{-3} Pa s^{-1}), specific humidity (*middle*, unit: g/kg), vorticity (*bottom*, unit: 10^{-5} s^{-1}) averaged over the South China box (107°E–120°E, 21°N–27°N) during strong (*left*) and weak (*right*) ISO years.

Lagged day 0 denotes a time when the ISO rainfall anomaly reaches maximum over South China. Areas exceeding the 95 % confidence level were *shaded*

China were investigated based on the analysis of station rainfall and NCEP reanalysis data. Two dominant sub-seasonal variability modes in South China are identified, one with a quasi-biweekly period (10–20 days) and the other with an intraseasonal period (20–60 days). There are

high positive correlations between the summer precipitation anomaly and the intensity of the QBW and ISO modes. The correlation coefficients are 0.78 and 0.74 respectively for the period of 1958–2007, which exceed a 99 % confidence level.
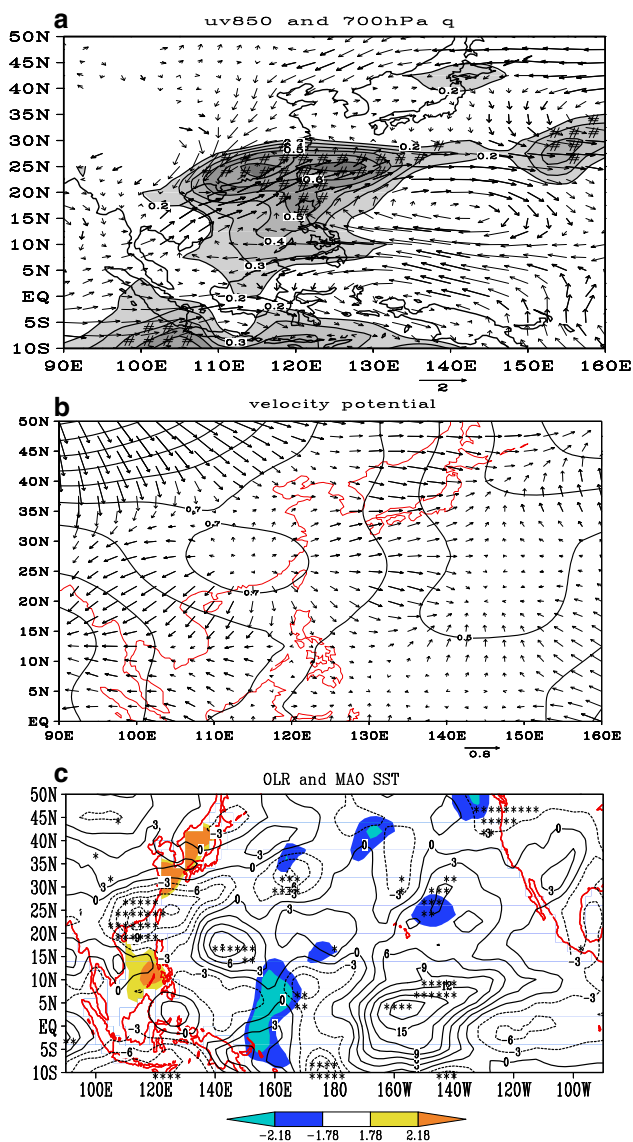
Fig. 12 The composite differences (wet minus dry years) of (**a**) 850 hPa wind (vector, unit: m s^{-1}, the difference exceeding a 95 % confidence level was plotted) and specific humidity at 700 hPa (contour, unit: g/kg, regions exceeding a 95 % confidence level were marked by #), **b** 200-hPa velocity potential (unit: 10^6 m^2 s^{-1}, *dark vectors* denote that the difference exceeds a 95 % confidence level), and (**c**) OLR (contour, unit: w/m^2, *asterisk* denotes where the difference exceeds a 95 % confidence level) and SST (*shaded*, unit: °C). A student t test was applied for checking the statistical significance. In (**c**), *blue* and *yellow* (*green* and *orange*) denote the SST differences exceeding a 90 % (95 %) confidence level

The composite structure and evolution characteristics of the QBW and ISO modes were examined. It is found that the QBW and ISO modes bear many similarities in the horizontal structure. For example, vorticity perturbations associated with the two modes exhibit a similar northwest–southeast oriented wave train pattern. The vorticity and rainfall signals associated with the two modes propagate northwestward, despite of their different phase speeds. The two modes exhibit the same baroclinic vertical structure.

The most evident difference between the QBW and ISO modes lies in the amplitude and latitudinal/longitudinal extent. While low-level moisture phase leading to convection appears in both the strong and weak QBW composites, such a phase leading only occurs in the strong ISO composite, not in the weak ISO composite.

The possible role of the mean state in regulating the QBW/ISO mode strength was investigated. It was found that when South China is anomalous wet, large-scale atmospheric conditions over the QBW/ISO development region (including the South China Sea and the Philippine Sea) are characterized by deeper moist layer, convectively more unstable stratification, and greater ascending motion. It is argued that these large-scale environmental conditions favor the amplification of the QBW and ISO perturbations. Therefore, the observed high positive correlations between the summer precipitation anomaly and the intensity of the sub-seasonal modes arise from the large-scale control of the background mean flow.

Previous studies (e.g., Yang et al. 2002; Inoue and Matsumoto 2004; Wu et al. 2005) suggested that there is unrealistic interdecadal variability in the NCEP reanalysis. To test whether or not such an interdecadal bias may contaminate the aforementioned interannual relationship, we conducted a parallel analysis using ERA-40 reanalysis dataset. It was found that the composite QBW/ISO structure and evolution characteristics obtained from the ERA40 dataset resemble well those derived from the NCEP reanalysis (figure not shown), confirming that the in-phase relationship between the mean state and the sub-seasonal modes is robust.

Previous works mainly focused on the climatological feature of the QBW and ISO modes, whereas the current study examines how the QBW/ISO mode structure and evolution characteristics alter on the interannual timescale and what causes such a change. Several works (e.g., Wang and Xie 1997; Chatterjee and Goswami 2004; Li and Zhou 2009) have discussed the possible origins of the QBW and ISO modes in the tropics. Here we hypothesized that the interannual variation of the sub-seasonal modes is attributed to the change of the mean state, in particular the background low-level moisture field. This is physically reasonable because the tropical low-frequency modes are often associated with convective heating. A favorable mean state with higher relative humidity in lower-to-middle troposphere would promote a stronger perturbation heating and thus stronger amplitude of the QBW/ISO modes. This large-scale control argument is supported by the observational fact that there is a high correlation between the mean state and the perturbations (as shown in Fig. 3). A further numerical model study is needed to understand the relative
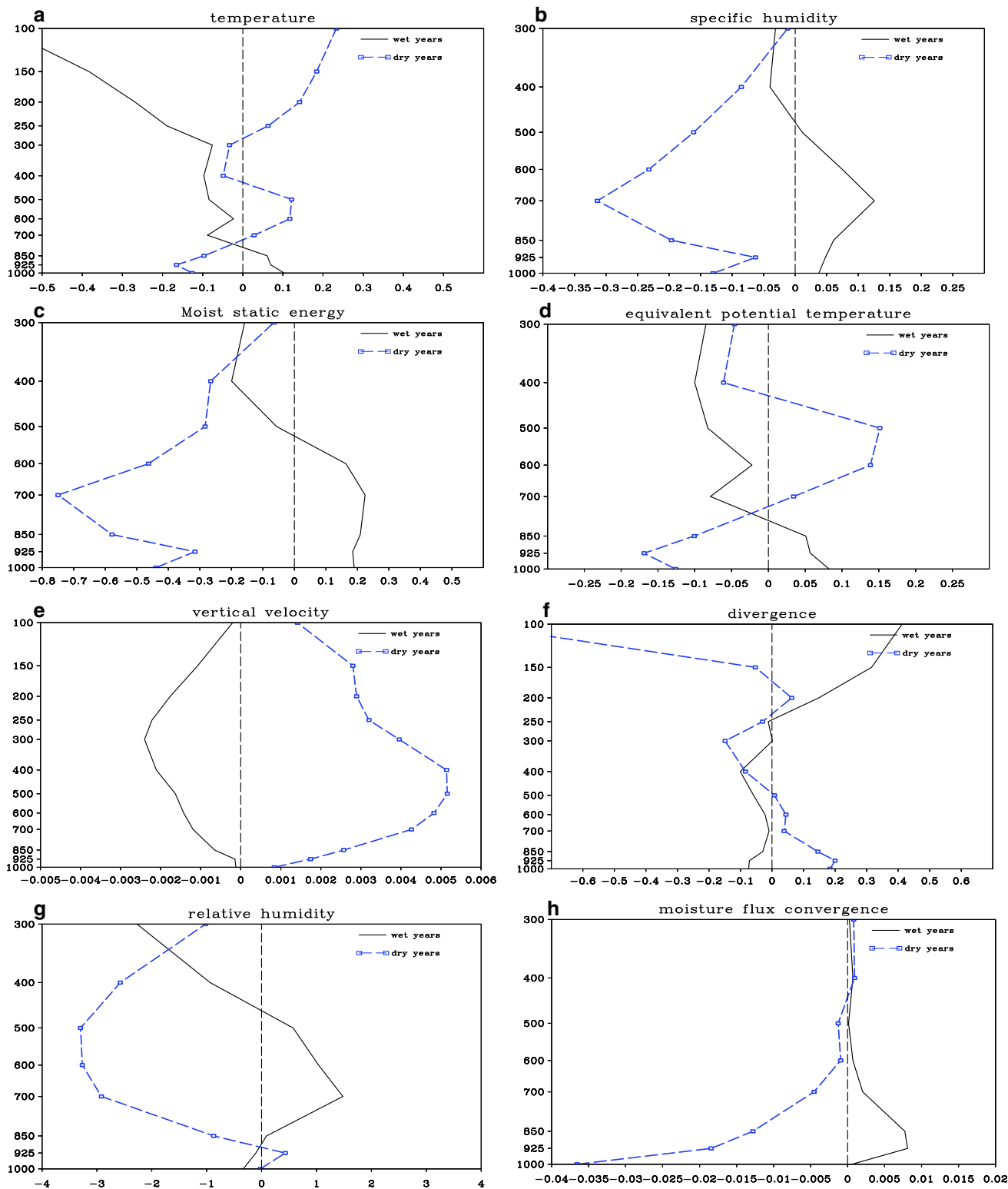
Fig. 13 Figure 12 Vertical profiles of (**a**) temperature (unit: °C), **b** specific humidity (unit: g/kg), **c** moist static energy (unit: J kg^{-1}), **d** equivalent potential temperature (unit: K), **e** vertical velocity (unit: Pa s^{-1}), **f** divergence (unit: 10^{-6} s^{-1}), **g** relative humidity (unit: %), and **h** moisture flux convergence (unit: g kg^{-1} s^{-1}) averaged over the key QBW and ISO activity region (110°–130°E, 10°–25°N). The climatologic mean profiles averaged over the 50 years have been removed. The *solid* (*dashed*) *curves* denote the composite for the wet (dry) years

roles of dynamic and thermodynamic fields of the mean state in affecting the QBW/ISO perturbations.

It is worth mentioning that the separation line between the QBW and ISO modes in Fig. 2 is not clearly defined. Such a separation may depend on variable, region, domain size, and period used. Nevertheless, many previous studies using different variables with different periods pointed out the existence of the QBW and ISO modes (e.g., Krishnamurti and Ardanuy 1980; Chen and Murakami 1988; Chen and Chen 1995; Annamalai and Slingo 2001; Hsu and Weng 2001; Kemball-Cook and Wang 2001; Lawrence and Webster 2002; Hsu et al. 2004; Mao and Chan 2005; Kajikawa and Yasunari 2005; Yang et al. 2008), suggesting that they are physical modes.

It is also worth mentioning that even though the in-phase relationship revealed in Fig. 3 is statistically significant, there is a mismatch between the mean state and the intensity of the ISO/QBW modes in some years. For example, in 1975 and 1991 the mean rainfall in South China was either wet or dry, but QBW/ISO intensity was normal. This indicates that the in-phase relationship between the mean and perturbation is not perfect (even though such a relationship is hold for most of the years). Thus, a caution is needed in applying the relationship to real-time prediction.

References

Annamalai H, Slingo JM (2001) Active/break cycles: diagnosis of the intraseasonal variability of the Asian summer monsoon. Clim Dyn 18:85–102

Bingham C, Godfrey MD, Tukey JW (1967) Modern techniques of power spectrum estimation. IEEE Trans Audio Electroacoust AU-15:56–66

Cai X-Z, Xu J-J, Wu B (2000) The canonical flood/drought during the pre flood season in South China and its some physical factors during earlier stage (in Chinese). Diagnostic analysis and prediction method research of severe flood and drought. Sun A-J, Wu G-X, Li Y-K, chief editor, Beijing meteorological publishing house (in Chinese), pp 166–173

Chang C-P, Zhang Y-S, Li T (2000a) Interannual and interdecadal variations of the East Asian summer monsoon and tropical Pacific SSTs Part I role of subtropic ridges. J Clim 13:4310–4325

Chang C-P, Zhang Y-S, Li T (2000b) Interannual and interdecadal variations of the East Asian summer monsoon and tropical pacific ssts. Part II: meridional structure of the monsoon. J Clim 13:4326–4340

Chatterjee P, Goswami BN (2004) Structure, genesis and scale selection of the tropical quasi-biweekly mode. Q J R Meteorol Soc 130:1171–1194

Chen T-C, Chen J-R (1995) An observational study of the South China Sea monsoon during the 1979 summer: onset and life cycle. Mon Weather Rev 123:2295–2318

Chen T-C, Murakami M (1988) The 30–50 day variation of convective activity over the western Pacific Ocean with emphasis on the northwestern region. Mon Weather Rev 116:892–906

Deng L-P, Wang Q-Q (2002) On the relationship between precipitation anomalies in the first raining season (April–June) in South China and SST over offshore waters in China. J Trop Meteorol (in Chinese) 18:44–55

Gao B, Chen Q-J, Ren D-D (1999) Diagnostic analysis on the severe drought/flood for the beginning of flood season I Southern part of the south of Yangtze River valley and Northern South China. Q J Appl Meteorol (in Chinese) 10:219–226

Gill AE (1980) Some simple solutions for heat-induced tropical circulation. J Meteorol Soc Jpn 106:447–462

Gilman DL, Fuglister FJ, Mitchell JM Jr (1963) On the power spectrum of red noise. J Atmos Sci 20:182–184

Guo Q-Y, Sha W-Y (1998) Analysis of rainfall variability during the first rainy season in South China. Q J Appl Meteorol (in Chinese) 9(s1):9–15

Hsu PC, Li T (2011) Interactions between boreal summer intraseasonal oscillations and synoptic-scale disturbances over the western North Pacific. Part II: apparent heat and moisture sources and eddy momentum transport. J Clim 24:942–961

Hsu HH, Weng C-H (2001) Northwestward propagation of the intraseasonal oscillation in the western North Pacific during the boreal summer: structure and mechanism. J Clim 14:3834–3850

Hsu CH, Weng C-H, Wu C-H (2004) Contrasting characteristics between the northward and eastward propagation of the intraseasonal oscillation during the boreal summer. J Clim 17:727–743

Hsu PC, Li T, Tsou C-H (2011) Interactions between boreal summer intraseasonal oscillations and synoptic-scale disturbances over the western North Pacific. Part I: energetics diagnosis. J Clim 24:927–941

Inoue T, Matsumoto J (2004) A comparison of summer sea level pressure over East Eurasia between NCEP-NCAR reanalysis and ERA-40 for the period 1960–99. J Meteorol Soc Jpn 82:951–958

Kajikawa Y, Yasunari T (2005) Interannual variability of the 10–25- and 30–60-day variation over the South China Sea during boreal summer. Geophys Res Lett 32:L04710. doi:10.1029/2004 GL021836

Kemball-Cook S, Wang B (2001) Equatorial waves and air–sea interaction in the boreal summer intraseasonal oscillation. J Clim 14:2923–2942

Krishnamurti TN, Ardanuy P (1980) The 10 to 20 day westward propagating modes and breaks in the monsoons. Tellus 32:15–26

Lawrence DM, Webster PJ (2002) The boreal summer intraseasonal oscillation: relationship between northward and eastward movement of convection. J Atmos Sci 59:1593–1606

Li T, Wang B (2005) A review on the western North Pacific monsoon: synoptic-to-interannual variabilities. Terres Atmos Ocean Sci 16:285–314

Li T, Zhou C (2009) Planetary scale selection of the Madden-Julian oscillation. J Atmos Sci 66:2429–2443

Li Q-Y, Long Z-X, Li G-L (1995) Low frequency oscillation of tropical atmosphere in South China Sea associated with rainfall anomalies in early-summer in South China. A symposium for severe flood in South China in 1994, Beijing meteorological publishing house (in Chinese), 17–23

Li S-Z, Wen Z-P, Zhou W (2011) Long-term change in summer water vapor transport over South China in recent decades. J Meteorol Soc Jpn 89:271–282

Liang J-Y (1994) The interannual variations of the subtropical high ridge position over western Pacific in June and its influence on precipitation in South China. J Trop Meteorol (in Chinese) 10:274–279

Liang J-Y, Wu S-S (1999) Variation of rainfall anomalies in Guangdong associated with summer monsoon. J Trop Meteorol (in Chinese) 15:38–47

Liebmann B, Hendon HH, Glick JD (1994) The relationship between tropical cyclones of the Western Pacific and Indian oceans and the Madden-Julian oscillation. J Meteorol Soc Jpn 72:401–412

Lin A-L, Liang J-Y, Li C-H, Gu D-J, Zhen B (2007) Monsoon circulation background of '0506' continuous rainstorm in South China. Adv Water Sci (in Chinese) 18:424–432

Lu S-J (1990) Climate change in Guangdong (in Chinese). Beijing meteorological publishing house, pp 67–80

Mao J-Y, Chan JCL (2005) Intraseasonal variability of the South China Sea summer monsoon. J Clim 18:2388–2402

Qi Y, Zhang R, Li T, Wen M (2008) Interactions between the summer mean monsoon and the intraseasonal oscillation in the Indian monsoon region. Geophys Res Lett 35:L17704. doi:10.1029/2008GL034517

Qin W, Sun Z-B, Ding B-S, Zhang A-H (1994) Precipitation and circulation features during late-spring to early-summer flood rain in South China. J Nanjing Inst Meteorol (in Chinese) 17:455–461

Shi X-L, Ding Y-H (2000) A study on extensive heavy rain processes in South China and the summer monsoon activity in 1994. Acta Meteorologica Sinica (in Chinese) 55:666–678

Smith TM, Reynolds RW (2003) Extended reconstruction of global sea surface temperatures based on COADS data (1854–1997). J Clim 16:1495–1510

Smith TM, Reynolds RW (2004) Improved extended reconstruction of SST (1854–1997). J Clim 17:2466–2477

Trenberth KE (1984) Signal versus noise in the Southern Oscillation. Mon Weather Rev 112:326–332

Wang B, Xie X (1997) A model for the boreal summer intraseasonal oscillation. J Atmos Sci 54:72–86

Wang B, Wu R, Li T (2003) Atmosphere-warm ocean interaction and its impact on Asian-Australian monsoon variation. J Clim 16:1195–1211

Wen Z-P, Dong L-Y, Wu L-J (2007) The characteristics of 30–60 day oscillation and its relation to the durative rainstorm in Guangdong. Acta Scientiarum Naturalium Universitatis Sunyatseni (in Chinese) 46:98–103

Wu H-Q, Zhang A-H, Jiang B-R (1998) Relationship between the variation of Antartic Sea ice and the pre flood season rainfall in South China. J Nanjing Inst Meteorol (in Chinese) 21:266–273

Wu R, Kinter JL III, Kirtman BP (2005) Discrepancy of interdecadal changes in the Asian region among the NCEP-NCAR reanalysis, objective analyses, and observations. J Clim 18:3048–3067

Wu R, Wen Z, Yang S, Li Y (2010) An interdecadal change in southern China summer rainfall around 1992–93. J Clim 23:2389–2403

Wu R, Yang S, Wen Z, Huang G, Hu K (2012) Interdecadal change in the relationship of southern China summer rainfall with tropical Indo-Pacific SST. Theor Appl Climatol 108:119–133

Xue F, Wang H-J, He J-H (2003) The influence of Mascarene high and Australian high interannual variation on the summer precipitation in East Asia. Chin Sci Bull (in Chinese) 8:287–291

Yang S, Lau K-M, Kim K-M (2002) Variations of the East Asian jet stream and Asian-Pacific-American winter climate anomalies. J Clim 15:306–325

Yang J, Wang B, Wang B (2008) Anticorrelated intensity change of the quasi-biweekly and 30–50-day oscillations over the South China Sea. Geophys Res Lett 35:L16702. doi:10.1029/2008GL034449

Zhang A-H, Wu H-Q, Wu Q, Ren B-R (1997) The preliminary exploration for the influence of general circulation over Southern hemisphere on precipitation over south China during pre-flood season. Meteorol Mon (in Chinese) 23:9–15

Zhou C, Li T (2010) Upscale feedback of tropical synoptic variability to intraseasonal oscillations through the nonlinear rectification of the surface latent heat flux. J Clim 23:5738–5754